Hyperfine interactions of ^{111}In-implanted tin oxide thin films

1991 J. Phys.: Condens. Matter 3 3625

(http://iopscience.iop.org/0953-8984/3/20/023)

J. Phys.: Condens. Matter 3 (1991) 3625–3634. Printed in the UK

Hyperfine interactions of ^{111}In-implanted tin oxide thin films

M Renteria†, A G Bibiloni†, M S Moreno†, J Desimoni†, R C Mercader†, A Bartos‡, M Uhrmacher‡ and K P Lieb‡

† Departamento de Fisica, Facultad de Ciencias Exactas, Universidad Nacional de La Plata, c.c. No 67, 1900 La Plata, Argentina

‡ II. Physikalisches Institut der Universität Göttingen, Bunsenstrasse 7–9, D-W3400 Göttingen, Federal Republic of Germany

Received 13 December 1990

Abstract. Thin Sn–O films were prepared by thermal evaporation of high-purity tin in a low-pressure oxygen atmosphere. The films were monitored by conversion electron Mössbauer spectroscopy (CEMS). Radioactive $^{111}In^{+}$-ions were implanted into the films and perturbed angular correlation (PAC) measurements were carried out in air after different annealings up to 1023 K. Two phases were sufficient to describe the PAC data, which are attributed to SnO and SnO_2. The temperature dependence of these phases was found to agree with CEMS measurements on Sn–O films after similar annealing programmes.

1. Introduction

Thin transparent dioxide films—amorphous or crystalline—are of particular technological importance. In fact, they are used in many devices where transparent conductors are needed. Their optical and electrical properties depend on the crystalline state of the films. Since different phases coexist, microscopic analysing methods, such as perturbed angular correlation (PAC) and conversion electron Mössbauer spectroscopy (CEMS), are ideally suited to observe the evolution of these phases, i.e. the transformation from the amorphous to the crystalline state.

In the past the PAC technique has been applied to study SnO_2, using the $^{111}In/^{111}Cd$ hyperfine probe [1–4]. However, the interpretation of the observed hyperfine parameters in SnO_2 and their temperature dependence are still a matter of controversy. Wolf *et al* [1] diffused ^{111}In into SnO_2 powder at about 1300 K under argon-protective gas. In the temperature range between 4 and 1260 K they found a quadrupole interaction with frequency $\nu_Q = 116(1)$ MHz and an asymmetry parameter $\eta = 0.1(1)$, with the interaction split into a static and a dynamic part. At temperatures above 1000 K, the static component reached 75%. Probe decay after-effects due to unfilled inner electron shells were proposed to explain the observed temperature dependence.

During oxidation experiments with dilute (a few ppm) ^{111}InSn alloys the La Plata group [2] found two different environments for the ^{111}In probe atoms, characterized by $\nu_{Q1} = 109(4)$ MHz with $\eta_1 = 0.67(5)$ and $\nu_{Q2} = 226(5)$ MHz with $\eta_2 = 0.40(4)$. The same hyperfine parameters were seen after diffusion of ^{111}In into SnO_2 powder samples

0953-8984/91/203625+10$03.50

[3, 4], supplied by Wolf *et al* [1]. In these experiments the quadrupole frequency ν_{Q1} remained nearly constant, whereas the asymmetry parameter η_1 varied reversibly from 0.65 to 0.15 in the measured temperature range from 17 to 1073 K. As a possible explanation for the two components the trapping of a singly or doubly ionized oxygen vacancy at the probe atom was proposed [2–4]. Nevertheless, at high temperatures the PAC parameters of complex 1 in [2] and [4] were similar to those of the static component of [1].

The present study was performed to establish the hyperfine parameters of ^{111}Cd in the tin oxides. In several previous experiments it was shown that the *implantation* of ^{111}In into metal oxides (for example silver, copper, manganese etc.) followed by thermal annealing or a phase transition [5–8] leads to a high fraction of probes on substitutional sites. Typically, after the implantation only a smaller fraction of probes is found in a perfect environment, characterized by a sharp quadrupole frequency. Most of the probes show a broadly distributed frequency spectrum around the frequency typical for the perfect site. This observation can be easily explained by distant damage in the probe neighbourhood [8]. In fact, the 'sharp' fraction can be enhanced by annealing. Even more effective is a phase transition to another oxide (Redox reaction): When the oxide has reached its final crystalline phase, most of the probes are found on substitutional defect-free sites (see, for example, [6]). We applied the same technique and implanted ^{111}In into Sn–O films which afterwards were subject to an oxidation phase transition. After an appropriate thermal treatment the doped samples approached a crystalline transparent SnO_2 phase.

2. Experimental details

Thin tin oxide films were prepared by thermal evaporation of metallic tin (99.999% purity) in a low-pressure oxygen atmosphere (about 2×10^{-3} mbar) onto an optically polished quartz substrate. The rectangular plate was kept at about 300 K during evaporation. Rutherford backscattering analysis with 900 keV α-particles revealed a film thickness of less than 1000 nm. CEMS measurements performed before the $^{111}In^+$ implantation clearly showed the presence of two possible tin valence states, 2+ and 4+, as can be seen in figure 1 (top). The Göttingen heavy ion implanter IONAS [9] was used to implant a total dose of about 4×10^{12} ^{111}In ions of 400 keV into each sample. A thermal annealing programme was performed in air to eliminate possible radiation damage and to transform the material to the more stable SnO_2 phase. The samples were heated at 683 K for 15, 30 and 120 min and at 923 and 1023 K, each time for 15 min. After the annealing at 923 K the films became transparent, as expected for the SnO_2 phase.

All PAC spectra were taken at room temperature in a coplanar 90° arrangement of four 2 in × 2 in NaI(Tl) detectors. A conventional slow–fast coincidence circuit was used, as described in [10], which allows for high counting rates. Twelve 1 K coincidence spectra $C(\Theta, t)$ of all possible start–stop combinations of the four detectors were measured simultaneously, routed and stored in a 16 × 1024 channel 24 bit deep histogramming CAMAC (computer-aided measurement and control) memory [11], in order to exploit the full counting statistics available. With the eight $C(90°, t)$ and the four $C(180°, t)$ coincidence spectra the usual perturbation function $R(t)$ was calculated:

$$R(t) = 2\frac{C(180°, t) - C(90°, t)}{C(180°, t) + 2C(90°, t)} = A_{22}^{\text{eff}} \sum_{i=1}^{4} f_i G_{2i}(t). \tag{1}$$

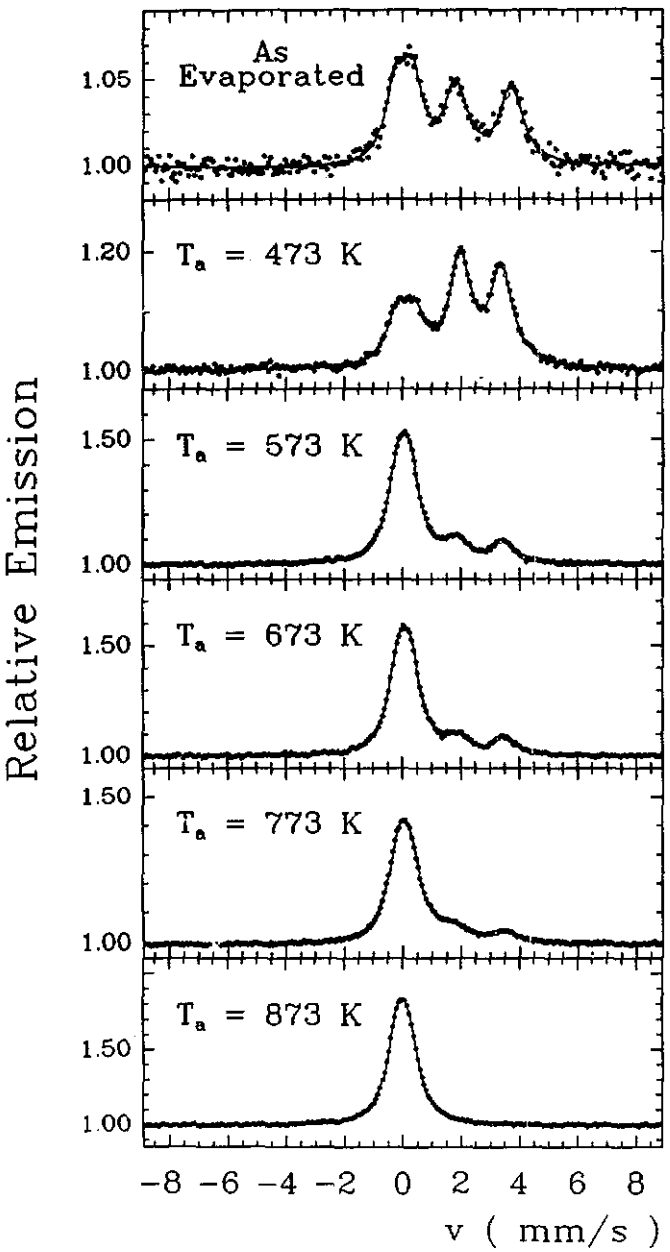

Figure 1. CEMS spectra of a Sn–O thin film, after successive isochronal (1 h) thermal annealing in air. The doublets of SnO (peaks at the right) gradually disappear. After the annealing at 873 K only the peak corresponding to the Sn^{4+} oxidation state remains.

Here A_{22}^{eff} is the effective coefficient and f_i denotes the normalized fractions of probes at the site i. In the fitting procedure a static perturbation factor was assumed for

each site:

$$G_2(t) = \sum_{n=0}^{3} S_{2n}(\eta)\cos(\omega_n(\eta,\nu_Q)t)\exp(-(g_n(\eta)\delta t)^2/2). \quad (2)$$

These are the standard expressions used in the PAC analysis to describe a static electric field gradient (EFG) tensor, i.e. the quadrupole coupling constant $\nu_Q = eQV_{zz}/h$, the asymmetry parameter $\eta = (V_{xx} - V_{yy})/V_{zz}$ and the width δ of the distribution in ν_Q. Q denotes the electric quadrupole moment [12] of the 'sensitive' $5/2^+$ state of ^{111}Cd. S_{2n} and g_n are known functions of η [13], and the transition frequencies ω_n are related to ν_Q and η via $\omega_n = g_n(\eta)\nu_Q$. The exponential in the expression G_2 (t) describes a Gaussian frequency distribution of the width δ around ω_n. To account for the finite time resolution of the apparatus (4.2 ns FWHM) an amplitude factor [14] $A_n(\omega_n) = S_{2n}^{\text{eff}}/S_{2n}$ was introduced in equation (2). More details can be found in [8].

Table 1. Comparison between CEMS parameters at room temperature (taken from [24]) and the results obtained from our samples after thermal annealing treatments at 473 and 873 K in air.

Sample	Linewidth (FWHM) Γ (mm s^{-1})	Isomer shift δ (mm s^{-1})	Quadrupole splitting Δ (mm s^{-1})
Crystalline $Sn^{2+}O$ (T_a = 473 K)			
Collins *et al* [24]	0.916(8)	+2.678(3)	1.360(10)
This work	0.855(16)	+2.659(6)	1.402(10)
Crystalline $Sn^{4+}O_2$ (T_a = 873 K)			
Collins *et al* [24]	0.965(16)	+0.004(3)	0.499(13)
This work	0.797(7)	−0.006(5)	0.404(6)

Table 2. EFG parameters of the different observed fractions. Each parameter set is the average over the fits of all perturbation functions taken during the different annealing treatments.

i	ν_{Qi} (MHz)	η_1	δ_i (%)	ω_{1i} (MHz)	Comments
1	117(1)	0.18(2)	5(1)	114(1)	Undisturbed SnO_2
2	86(3)	0.68(8)	21(3)	114(1)	Disturbed SnO_2
3	170(10)	0.60(10)	25(3)	215(3)	Disordered or
4	160(10)	0	18–4	150(3)	damaged phase of SnO

The Mössbauer spectra were recorded in a conventional constant acceleration spectrometer with backscattering geometry. A mixture of flowing He and natural gas was used in the electron detector. The calibration of the spectra was carried out against a 6 μm α–Fe absorber. The non-linearity was fitted with a second degree polynomial. Isomer shifts refer to a $CaSnO_3$ absorber. The 5 mCi $Ba^{119m}SnO_3$ Mössbauer source was kept at room temperature and was driven in a triangular waveform. The CEMS spectra were taken after each step of a 1 h isochronal annealing programme in air (see figure 1); table 1 shows the fitted parameters of the most relevant spectra in comparison with previous measurements, while table 2 summarizes the results of the PAC experiment.

3. Crystal structures of SnO and SnO_2

The crystal structure of the blue-black SnO was first reported by Moore and Pauling [15] from an x-ray powder structure determination. The proposed configuration was confirmed by recent neutron diffraction studies [16]. The bimolecular unit cell is tetragonal ($a = 3.8029(5)$ Å, $c = 4.8382(8)$ Å) with each Sn^{2+} ion placed in the apex of a regular square-pyramid, as shown in figure 2(a). All Sn–O distances equal 2.224(8) Å and two angles of 117.3° exist. Each oxygen ion is surrounded tetrahedrally by four metal ions. These positions give rise to a plate-like morphology where tin layers are separated by oxygen layers.

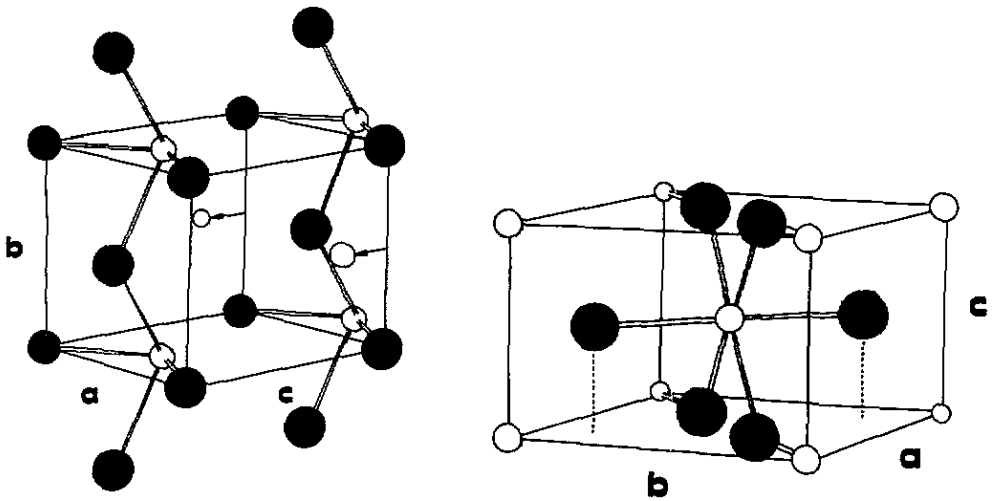

Figure 2. Simplified ball and stick model of the crystalline structures of (a) tin monoxide, SnO, and (b) tin dioxide, SnO_2. Black circles represent oxygen ions and white circles tin ions.

The SnO_2 has a rutile structure. Its symmetry is tetragonal with a flat unit containing two molecules. The cell dimensions are known from an x-ray single-crystal experiment [17] to be $a = 4.7373(1)$ Å, $b = 4.7368(2)$ Å, $c = 3.1862(1)$ Å, $\alpha = 89.999(3)°$, $\beta = 90.003(3)°$ and $\gamma = 90.002(3)°$. The Sn ions are octahedrally coordinated by the oxygen ions: each Sn^{4+} ion is placed at the centre of a distorted octahedron, all Sn–O distances being equal to 2.05 Å in the rectangular basal plane, as can be seen in figure 2(b). The Sn–O axial distance is longer than that of the basal plane, but does not differ by more than 0.01 Å. In both lattices the Sn ions occupy only one equivalent site, i.e. only a single EFG is expected, when the implanted ^{111}In probes reach substitutional lattice sites.

In ionic crystals the simple point charge model (PCM) often produces valuable estimations of the EFG tensor by summing all contributions of point charges located at the different lattice sites. These calculations predict the asymmetry parameter η of ^{111}Cd in oxides quite well [5–8, 18–22]. Making use of the ionic character of the tin oxides [23], we performed PCM calculations using the crystalline parameters from [16] and [17] for SnO and SnO_2, respectively. We found $\nu_Q(SnO) = 3.62$ MHz with $\eta(SnO) = 0$ and $\nu_Q(SnO_2) = 3.43$ MHz with $\eta(SnO_2) = 0.2$. The PCM coupling

constants ν_Q have to be multiplied by an 'anti-shielding' factor β to reproduce the experimental values.

4. Results and discussion

Even a quick inspection of figure 3, which displays the fitted PAC perturbation functions and the corresponding Fourier spectra, clearly reveals the development of a frequency triplet ($\omega_1 \simeq 110$ MHz) above annealing temperatures of 683 K, which finally dominates the Fourier spectrum at 1023 K. The CEMS data (figure 1, table 1) prove that, after a 1 h annealing in air at 873 K, only the Sn^{4+} ions (SnO_2 phase) are present in the film. As the same PAC parameters are found after diffusion of ^{111}In into SnO_2 [1], and also after oxidation of Sn, we conclude that these parameters ($\nu_{Q1} = 117$ MHz and $\eta_1 = 0.18$) characterize ^{111}Cd probes on substitutional cation sites in SnO_2. The predicted PCM asymmetry parameter $\eta_{PCM} = 0.2$ is also in good agreement with the data. In addition a second fraction f_2 is found with a broad frequency distribution centred around the same ω_1. This is a common observation in oxides [18] and is explained by distant defects which make the larger surrounding of the probe somewhat imperfect. In the actual evaporated thin film samples, an additional mechanism may be at work, as all PAC frequencies show a $\delta_{1-4} \geq 5\%$. Nevertheless, we assume that the sum of both fractions $f_1 + f_2$ represents the SnO_2 phase.

The PAC spectrum taken immediately after implantation is quite different. Such a pattern can be caused either by a radiation damaged neighbourhood of the probe or be a disordered SnO phase produced during the evaporation of the film. Indeed, after the implantation of the heavy In^+ ions, severe radiation damage often dominates the PAC spectra. It is seen as a broad distribution (δ up to 35%!). Such a distribution is, however, centred around a frequency ω_1 which is typical for ^{111}In on defect-free substitutional sites in crystalline samples [18]. Furthermore, an annealing cycle narrows this distribution. In the present experiment the broad distribution is centred around $\omega_1 = 180$ MHz, just in between the ω_1 values of the other two observed fractions (f_3 and f_4). So it may represent probes in *damaged* SnO material. On the other hand, this type of PAC perturbation function is also characteristic of a disordered region. The CEMS results may support this interpretation: after evaporation of the tin film both valence states are clearly found (see figure 1, top). But the hyperfine parameters fitted from this CEMS spectrum do not correspond to the values previously found for crystalline SnO and SnO_2 matrices. Furthermore, the relatively small effect and the line-broadening found here characterize disordered states, in agreement with previous experiments of Collins *et al* [24]. These phases should then correspond to positional disorder.

The unique identification of the SnO phase among the two additional observed fractions f_3 and f_4 in the PAC spectra is much more difficult. The only CEMS spectrum which shows the SnO crystalline values is the second spectrum of figure 1, measured after a 60 min annealing at 473 K. Up to 773 K the Sn^{2+} state can be seen. As the annealing was done successively, this state 'survived' at least 240 min of heating. The PAC spectrum at 923 K in figure 3 represents 135 min of cumulative heating, 120 min at 683 K and 15 min at 923 K. In this case it seems reasonable to conclude that both fractions are still present which may represent probes at SnO cation sites.

Fraction f_3 in the PAC spectra is characterized by $\nu_{Q3} = 171(10)$ MHz, $\eta_3 = 0.6(1)$ and a large distribution width $\delta_3 \simeq 25\%$. Note that this fraction varies dramatically

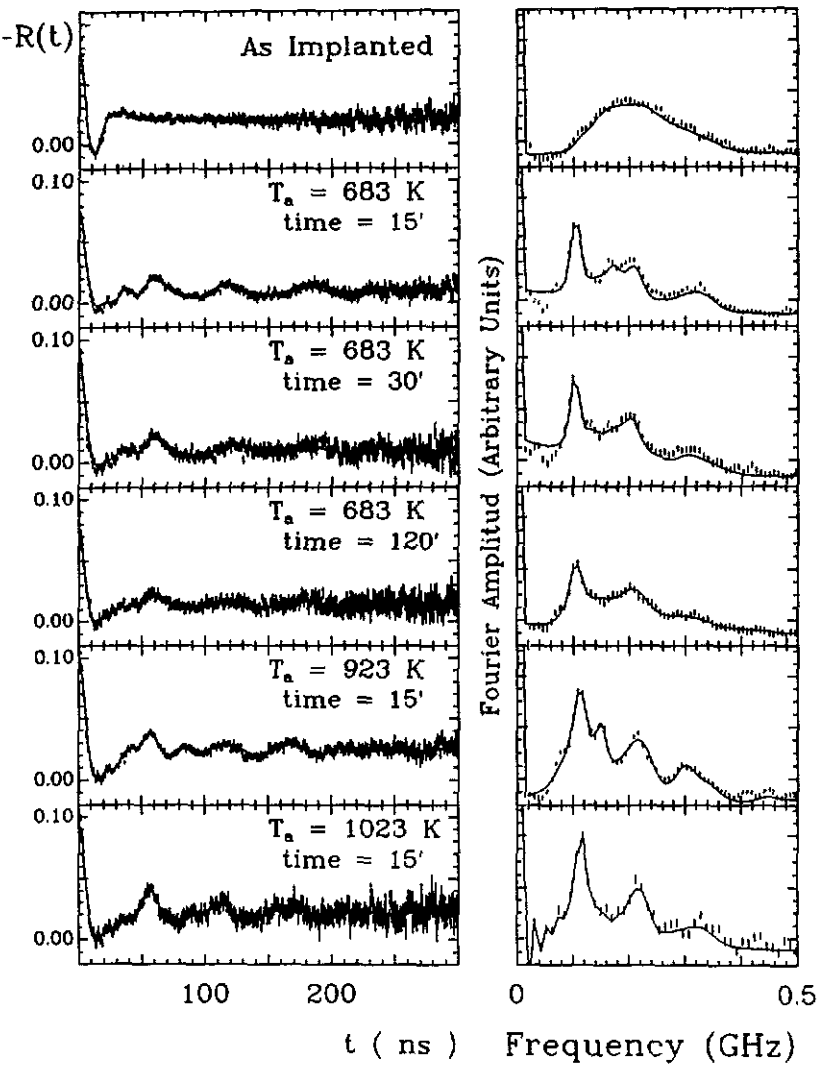

Figure 3. PAC and the corresponding Fourier spectra measured at room temperature after the successive thermal annealings indicated. The full lines are fits to the data.

from $f_3 = 85$ to 11%. Furthermore, the value of the asymmetry parameter η_3 is in conflict with the expected axially symmetric EFG ($\eta = 0$) in the SnO lattice structure. Calculations by Forker [25] predict an increasing asymmetry parameter η for increasing width δ. But the large value of η_3 is hard to extrapolate to $\eta_3 \to 0$ for $\delta_3 \to 0$. This micro-environment starts from damaged or disordered SnO after the implantation, as previously outlined. Therefore f_3 may represent probes in a disordered SnO-phase, still after some annealing.

About 10% of the probes (f_4) sense an EFG with axial symmetry ($\eta_4 = 0$) and a quadrupole frequency in the range $\nu_{Q4} = 160$–170 MHz. The constancy of the asymmetry parameter together with the varying coupling constant can be explained in terms of a model related to the SnO $\to$ SnO_2 transformation: the Sn^{2+} ion in the

vertex position of the Sn–O tetrahedron (see figure 2(*a*)) moves along the pyramid axis until it reaches the centre of its base, thus transforming to the octahedral coordination of the SnO_2 phase (see figure 2 (*b*)). Although both fractions f_3 and f_4 seem to be related to the SnO phase, we cannot correlate one of them to an undisturbed SnO cation site. To demonstrate the annealing behaviour of the film the summed fractions f_1+f_2 (Sn^{4+}) and f_3+f_4 (Sn^{2+}) are plotted in figure 4. The insert displays the CEMS fractions of the tin oxidation states. They were calculated from the fitted areas of the (2+) and (4+) peaks in the CEMS spectra with the help of the known resonant fraction of both states in the crystalline matrices of SnO and SnO_2, respectively. The same crystalline factor $f^{4+} = 0.6$ was assumed for the 573, 673 and 773 K CEMS spectra. There is good overall agreement between the CEMS and PAC fractions, except for the fact that, after a series of annealings, Sn^{2+} is still present in the PAC experiment, whereas in CEMS it has disappeared above 773 K. However, the different total heating time may explain this difference.

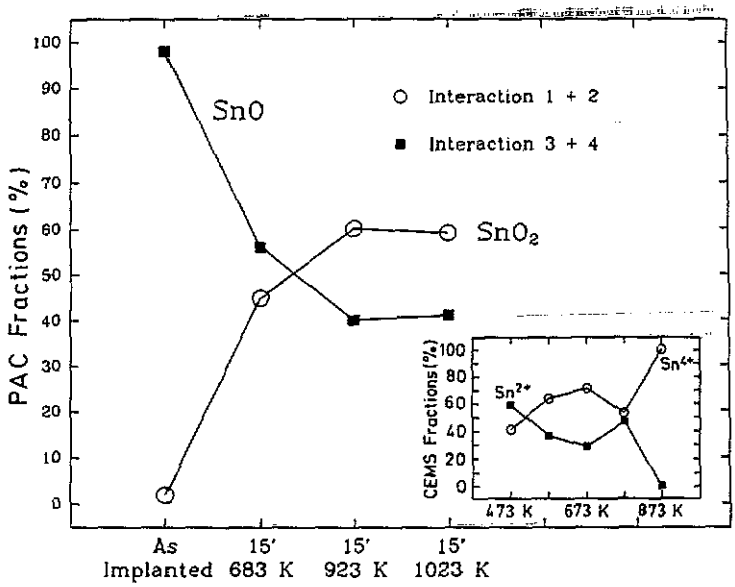

Figure 4. Evolution of the relative PAC fractions f_1+f_2 and f_3+f_4 as a function of the annealing treatments. For comparison, the evolution of the CEMS fractions is shown in the inset.

Finally, the hyperfine parameters of ^{111}Cd in the semiconductor SnO_2 allow the calculation of the 'anti-shielding' factor $\beta = \nu_Q(\text{exp})/\nu_Q(\text{PCM})$. This factor was found to depend on the nearest-neighbour (NN) oxygen coordination [26], increasing with the number of NN oxygen ions. The value β (SnO_2) = 34 is very close to that of the six-fold oxygen coordination in the bixbyite structure β (In_2O_3) = 35 [5] and is also close to the $\beta = 29.27$ usually adopted for ^{111}Cd in any matrix [27].

5. Conclusions

By means of two independent hyperfine interaction techniques (PAC and CEMS) we found that in thin films prepared under the present conditions two oxidation states

of Sn coexist, namely Sn^{2+} and Sn^{4+}. Furthermore, the initially disordered SnO and SnO_2 phases are transformed into the SnO_2 crystalline phase by an appropriate annealing treatment. The hyperfine parameters of ^{111}Cd in crystalline SnO_2, ν_Q = 117(1) MHz and $\eta = 0.18(2)$, were determined, confirming the results reported by Wolf *et al* [1]. These parameters agree with those found in [2–4], for one of the reported interactions at high temperatures. Although the hyperfine interaction parameters of ^{111}Cd in an undisturbed SnO environment could not definitely be characterized, our results support the assumption of 'good' SnO only developing in the film within a small window of annealing conditions.

Acknowledgments

The authors are indebted to Th Weber for the Rutherford backscattering analysis of the films and to Dr W Bolse for many discussions. One of the authors (MR) is grateful to Dr C P Massolo for much support and the careful reading of the manuscript. Helpful comments on the experiment by Dr A F Pasquevich are kindly acknowledged.

This work was partially supported by the Consejo Nacional de Investigaciones Cientificas y Tècnicas (CONICET), by the Stiftung Volkswagenwerk and the Kernforschungszentrum Karlsruhe, Federal Republic of Germany.

References

[1] Wolf H, Deubler S, Forkel D, Foettinger H, Iwatschenko-Borho M, Meyer M, Renn M and Witthuhn W 1986 *Mat. Sci. Forum* **10–12** 863
[2] Desimoni J, Bibiloni A G, Mendoza-Zelis L A, Damonte L C, Sanchez F H and Lopez-Garcia A 1987 *Hyperfine Interact.* **34** 271
[3] Bibiloni A G, Desimoni J, Massolo C P and Renteria M 1988 *Phys. Rev.* B **38** 20
[4] Moreno M S, Bibiloni A G, Massolo C P, Desimoni J and Renteria M 1989 *Phys. Rev.* B **40** 2546
[5] Bolse W, Uhrmacher M and Kesten J 1987 *Hyperfine Interact.* **35** 981
[6] Bartos A, Bolse W, Lieb K P, and Uhrmacher M 1988 *Phys. Lett.* **130A** 177
[7] Wiarda D, Bartos A, Lieb K P, Uhrmacher M and Wenzel T 1990 *25th Zakopane School of Physics* ed J Stanek (Singapore: World Scientific) at press
[8] Bolse W, Uhrmacher M and Lieb K P 1987 *Phys. Rev.* B **36** 1818
[9] Uhrmacher M, Pampus K, Bergmeister F J, Purschke D and Lieb K P 1985 *Nucl. Instrum. Methods* B **9** 234
[10] Arends A R, Hohenemser C, Pleiter F, de Waard H, Chow L and Suter R M 1980 *Hyperfine Interact.* **8** 191
[11] Schröder H, Bolse W, Uhrmacher M, Wodniecki P and Lieb K P 1986 *Z. Phys.* B **65** 193
[12] Herzog P, Freitag K, Reuschenbach M and Walitzki H 1980 *Z. Phys.* A **294** 13
[13] Kajfosz J 1973 *Institut of Nuclear Physics (Cracow) Report No 858/PM* unpublished
[14] Rogers J D and Vasquez A 1975 *Nucl. Instrum. Methods* **130** 539
[15] Moore W J and Pauling L 1941 *J. Am. Chem. Soc.* **63** 1392
[16] Pannetier J and Denes G 1980 *Acta Crystallogr.* B **36** 2763
[17] Hazen R M and Finger L W 1981 *J. Phys. Chem. Solids* **42** 143
[18] Bolse W, Bartos A, Kesten J, Uhrmacher M and Lieb K P 1989 *Ber. Bunsenges. Phys. Chem.* **93** 1285
[19] Bibiloni A G, Massolo C P, Desimoni J, Mondoza-Zelis L A, Sanchez F H, Pasquevich A F, Damonte L and Lopez-Garcia A R 1985 *Phys. Rev.* B **32** 2393
[20] Massolo C P, Renteria M, Desimoni J and Bibiloni A G 1988 *Phys. Rev.* B **37** 4743
[21] Requejo F, Bibiloni A G, Massolo C P, Renteria M and Desimoni J 1989 *Phys. Status Solidi* a **116** 503

[22] Renteria M, Wiarda D, Bibiloni A G and Lieb K P 1990 *Hyperfine Interact.* **60** 679
[23] Ladd M F C 1964 *Acta Crystallogr.* A **25** 486
[24] Collins G S, Kachnowski T, Benczer-Koller N and Pasternak M 1979 *Phys. Rev.* B **19** 1369
[25] Forker M 1973 *Nucl. Instrum. Methods* **106** 121
[26] Kesten J, Bolse W, Lieb K P and Uhrmacher M 1990 *Hyperfine Interact.* **60** 683
[27] Feiock F D and Johnson W R 1969 *Phys. Rev.* **39** 187